Chemical Engineering & Processing: Process Intensification 222 (2026) 110745

Contents lists available at ScienceDirect

Chemical Engineering and Processing - Process Intensification

journal homepage: www.elsevier.com/locate/cep

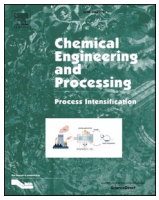

Towards energy-efficient spray drying: Geometric optimization of an ACLR nozzle for atomizing concentrated feeds

Miguel Ángel Ballesteros Martínez [a,*], Benedikt Heider [a], Volker Gaukel [b]

[a] Institute of Process Engineering in Life Sciences: Food Process Engineering, Karlsruhe Institute of Technology, Kaiserstraße 12, 76131 Karlsruhe, Germany
[b] Institute of Food Technology and Bioprocess Engineering, Max Rubner-Institut, Federal Research Institute of Nutrition and Food, 76131 Karlsruhe, Germany

ARTICLE INFO

Keywords:
ACLR nozzle
CFD
Geometrical optimization
Flow instabilities
Spray drying

ABSTRACT

Spray drying is a key method for large-scale production of food powders but remains among the most energy-intensive processes in the food industry. Increasing the solids content of liquid feeds can lower thermal energy demand; however, higher viscosities complicate atomization. The Air-Core-Liquid-Ring (ACLR) nozzle presents a promising approach, as it enables atomization of viscous feeds at low pressures (<0.8 MPa) and low air-to-liquid ratios (<1). Nevertheless, existing ACLR designs suffer from internal flow instabilities, leading to fluctuations in liquid lamella thickness and broad droplet size distributions. This study applies a validated CFD model to systematically investigate the influence of key geometric parameters on lamella stability for feeds with up to 54% wt. dry matter (1.33 Pa·s viscosity). The results indicate that a shorter outlet length, a larger chamber inclination, and rounded internal edges promote thinner and more stable lamellas. An optimized design incorporating these features was manufactured and experimentally evaluated, yielding a narrower droplet size distribution than the reference design, even at operating pressures and air-to-liquid ratios reduced by 40%. These findings demonstrate the energetic (of up to 45% when compared to a pressure-swirl nozzle) and operational savings when applying the ACLR nozzle at industrial scale.

1. Introduction

An important area of research in process engineering is how to intensify processes with the objective of reducing energy consumption and increasing efficiency. This topic of research becomes even more important, when energy prices generally continue to rise, like in the European Union [1]. Looking at the food industry, drying processes are known to be the most energy-consuming type of unit operation, being responsible for around 12–25 % of the total industrial energy consumption in many developed countries [2]. From this, it can be noticed that drying processes are an important target for process intensification.

At least when it comes to food powders, most products available on the market are produced using a spray dryer [3]. A straightforward way to reduce energy consumption is to increase the dry-matter content that can be fed to the atomizer. According to a model calculation on industrial spray drying by Fox et al. [3], an increase in feed dry matter content by 1 % can lead to a decrease in thermal energy consumption of the spray dryer by 3.8 %. However, a high dry-matter content also leads to a steep increase in feed viscosity, which makes atomization more difficult [4].

Consequently, it is vital that an appropriate nozzle design is selected that can handle those high viscosities. In general, pneumatic nozzles, both external and internal mixing, are considered appropriate to handle feeds with high viscosities, and each have their advantages and disadvantages. External-mixing nozzles allow the independent adjustment of the air and liquid flow, enabling a better adjustment of the air-to-liquid ratio (ALR) and of the resulting droplet sizes [5,6]. However, internal-mixing atomizers usually require lower gas rates, in comparison to external-mixing atomizers [7]. For example, Stähle et al. [8] showed than an internal-mixing nozzle, in that case, an effervescent nozzle, requires only 30–50 % of the gas mass flowrate of external-mixing ones to achieve similar Sauter mean diameters. A lower atomizing gas flowrate leads to reduced operating costs and should lead to a higher heat transfer efficiency inside the drying tower, because of the lower amount of atomization air necessary [9].

One promising nozzle design is the Air-Core-Liquid-Ring (ACLR) nozzle, which is a type of internal-mixing pneumatic nozzle [10]. The nozzle is based on injecting a high-speed gas flow at the center of a flowing liquid feed. Such a design favors the development of an annular flow inside the nozzle, with an air core surrounded by a liquid film, also

* Corresponding author.
E-mail address: miguel.ballesteros@kit.edu (M.Á. Ballesteros Martínez).

https://doi.org/10.1016/j.cep.2026.110745
Received 24 October 2025; Received in revised form 7 February 2026; Accepted 9 February 2026
Available online 10 February 2026

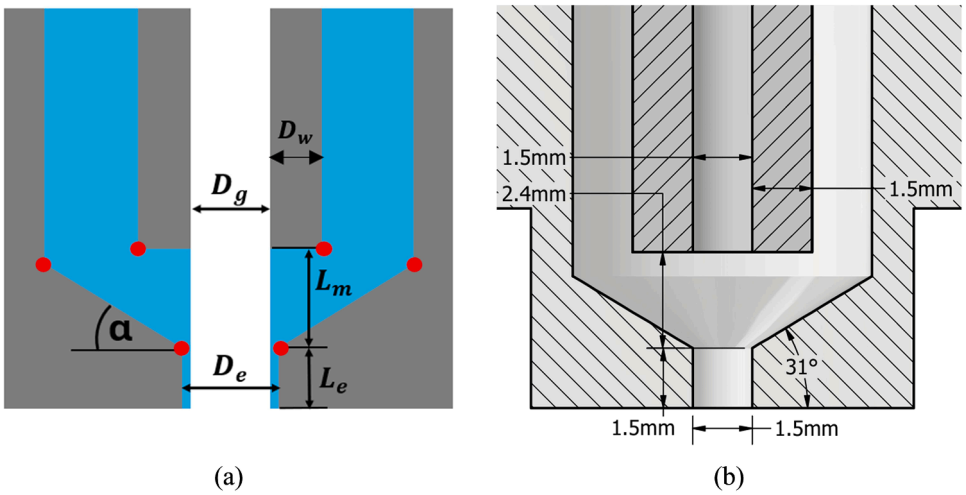

Fig. 1. (a) Schematic of all the different geometrical parameters identified for the ACLR nozzle. The red circles indicate the edges that can be rounded off. (b) Diagram showing the dimensions of the base nozzle geometry.

Table 1
Summary of important geometrical parameters of the nozzle, indicating whether they have already been investigated, and what their influence on the internal flow is. The underlined values represent the values of the base ACLR nozzle geometry.

Geometrical parameter	Expected/known influence on internal nozzle flow	Already investigated
D_g	Smaller D_g causes larger pressure loss and higher initial velocity for the gas, which should reduce the lamella thickness.	—
L_m	Longer L_m means larger free surface, leading to more flow instabilities, but smaller L_m means smaller flow area available for the liquid, leading to higher pressure losses.	Larger temporal unsteadiness of the Sauter mean diameter (SMD) → Evaluated at <u>2.4</u>, 7.4, and 12.4 mm [10].
L_e	Longer L_e means larger free surface, leading to more flow instabilities, but also some length is needed so that the annular flow can develop.	SMD and its standard deviation are larger with longer outlet channels → Evaluated for an effervescent nozzle at <u>1.5</u>, 3, 4.5, and 6 mm [22].
D_e	Smaller D_e means less available area for the annular flow and, with it, larger pressure losses and phase velocities. The larger gas velocity might lead to thinner liquid lamellas.	Scaling the nozzle up while keeping the same ALR increases the SMD → Evaluated for <u>1.5</u> and 3 mm [23].
D_w	The thinner the D_w, the more area for the liquid to flow through, and, with it, the smaller the liquid velocity. This might reduce turbulence, and with it, the flow instabilities.	—
α	A higher α means that the change of direction of the liquid, as it mixes with the air flow, is smoother. In turn, this should cause the annular flow that forms to be smoother and more stable.	—
R	The larger the rounding R, the smoother the change of direction of the flow as it encounters a corner, which should lead to a smoother and more stable annular flow.	—

called a liquid lamella [11]. The performance of the ACLR nozzle has been so far proven to successfully operate even for viscosities up to 3 Pa•s and dry-matter concentrations up to 57 % wt [12]., at pressures of barely 0.7 MPa and ALR below 1. These operating requirements are small in comparison to the pressure requirements of pressure swirls, 5–25 MPa [13], and air flow requirements of external-mixing nozzles, with ALRs of 1–15 [14]. Moreover, the ACLR can handle much higher dry-matter contents (52–57 % wt [12].) compared to standard pressure swirl nozzles, which are typically limited to a maximum of 30 % wt [15]. at the lab scales evaluated. Based on energy estimates from Fox [3], this increase in atomizable dry-matter content could result in energy savings of up to 45 %.

However, at the conditions evaluated, flow instabilities tend to develop in the annular flow inside the nozzle. This unstable flow behavior is in fact a common problem with internal-mixing nozzles [16, 17]. It is important to clarify that, in this context, flow instabilities refer to fluctuations of the annular flow inside the nozzle, most notably oscillations in the thickness of the liquid lamella (as evidenced in Section 6). These fluctuations lead to a broader droplet size distribution and an increased proportion of large droplets with diameters above 500 μm [18]. It should be distinguished from the microscopic instability mechanisms, such as Kelvin-Helmholtz instabilities, which are responsible for the actual breakup and atomization of the liquid [19]. Here, flow instabilities denote the oscillations in the liquid lamella, which need to be addressed by either evaluating higher operating pressures, or by improving the nozzle geometrical design.

While the effect of the operating pressure, and in general, of the ALR, on the lamella thickness and the resulting droplet sizes has already been identified [18], the effect of the geometrical design of the nozzle has not yet been systematically investigated. The present study encompassed two complementing objectives. On the one hand, to identify and vary the geometrical parameters of the nozzle design that have a positive effect on reducing the internal flow instability. On the other hand, to find the combination of the different geometrical parameters that most improve the flow stability and, with that, produce the most stable spray with smaller droplets. Experimentally evaluating numerous geometrical variations would be wasteful and time consuming, so the geometrical analysis contained in this study was conducted numerically, utilizing an implemented CFD model of the nozzle that has already been validated with experimental data for feed viscosities up to 1.33 Pa·s [20]. Although the geometrical variations were evaluated using a validated numerical model, we also compared the droplet size distribution (DSD) of the optimized nozzle with that of the base nozzle design, using a spray test rig.

Table 2
Simulation plan for the geometrical analysis. The underlined values represent the values of the base geometry.

Geometrical parameter	Variation level			
$\mathbf{D_e}$ [mm]	0.8	1.2	<u>1.5</u>	
$\mathbf{L_e}$ [mm]	0.8	1.2	<u>1.5</u>	
α [°]	<u>31</u>	45	60	
$\mathbf{D_w}$ [mm]	0.9	1.2	<u>1.5</u>	
R [mm][a]	0.5	1	4	5

[a] In the base geometry, there were only sharp corners, so there was no original rounding radius.

2. Geometrical analysis

The main geometrical parameters of the nozzle that are assumed to have an influence on the flow stability are shown in Fig. 1a. These main parameters are: the diameter (D_g) and wall thickness (D_w) of the gas capillary, the length (L_m) and inclination (α) of the mixing chamber, and the length (L_e) and diameter (D_e) of the outlet channel. Additionally, we considered the possibility of rounding off the sharp internal edges of the nozzle, indicated in Fig. 1a with red circles. In that case, the actual rounding radius (R) is also a geometrical parameter to consider. To give a better reference of the scale of these parameters, all the important dimensions of the nozzle geometry are shown in Fig. 1b.

Some of these parameters had been already investigated by previous studies about the ACLR nozzle, or at least about pneumatic nozzles. For those parameters that had not yet been investigated, we considered which factors could favor the formation of a stable annular flow inside the nozzle. Table 1 shows the summarized information about previous studies and the expected, or in some cases, already known, effects of the geometrical parameters on the internal flow. In principle, the considered parameters could have one of three possible effects. First, they could reduce the contact time or the free surface between the phases, which might give the instabilities less time to develop. This is the case for L_m or L_e. Second, they reduce the angle at which the two phases impinge on each other. In turn, that reduces the apparition of oscillations in the interface. This is the case for α or for rounded edges with a given R. Third, they might affect the relative velocity between the phases, which is one of the driving forces for the apparition of instabilities [21]. This is the case for D_g, D_w, or D_e.

With the information gathered in Table 1, we preemptively discarded parameters that had already been sufficiently investigated by previous studies about the ACLR nozzle, such as the L_m. Additionally, we decided to keep the diameter of the capillary (D_g) and the total width of the nozzle constant, because changing them would simply affect the inlet pressure loss and/or volume flow of the phases, which would correspond to scaling up the nozzle or simply increasing the ALR. With that in mind, five parameters were selected for the geometrical analysis: the dimensions of the nozzle outlet channel, L_e and D_e, the parameters that can change the impingement angle between the phases, α and R, and, finally, the D_w.

2.1. Simulation plan for geometrical analysis

For most of the selected geometrical parameters, we chose two alternative values, different than the base value in the base design. These values are shown in Table 2. The exception to this is the edge rounding, where we instead considered four different rounding radii. In total, 12 simulations needed to be carried out.

Based on the geometrical analysis results, we proposed an improved nozzle design, which was evaluated and compared with the base geometry. Every geometrical variation consisted of the base nozzle geometry with a single parameter being altered at a time. Appendix A details the specifics of how every variation of the nozzle geometry was generated.

3. Spray test rig

All experiments were carried out in a spray test rig, which has been described in detail in a previous study [24]. In short, it is composed of a closed cabin with a vertical atomizer on top. The liquid flow is supplied by an eccentric screw pump and measured by a gear flow meter. Air is supplied by a compressor. The air pressure is adjusted with a pressure regulator, and its resulting volume flow is measured by a gas flow meter.

The DSD was measured using a laser diffraction spectroscope (Spraytec, Malvern Instruments, Malvern, UK). It was equipped with a 750 mm focal lens, offering a droplet size measuring range of 2–2000 μm, and it was located 35 cm below the nozzle exit. This distance was chosen based on previous experimental testing [12]. The laser beam crossed the full cone spray angle at the nozzle axis centerline. The measurement was conducted at a frequency of 10 kHz over a time of 1 s, leading to 10,000 DSDs. Each recorded distribution had to be corrected from the beam-steering effect. This effect is a systematic error that is especially prevalent in pneumatic nozzles. It causes the apparent detection of large spray droplets due to density gradients in the gas phase. The correction was done by adapting the code developed by Wittner et al. [25]. In order to characterize the width of the droplet distributions, we tracked the 10 %, 50 % and 90 % volumetric percentiles of the measured sizes, which are denoted as $x_{10,3}$, $x_{50,3}$, and $x_{90,3}$, respectively. As will be discussed in more detail during the analysis of the results, the presence of large droplets represents the most significant limitation for the application of the ACLR in industrial processes. The reason for this is that large droplets can cause several issues during operation, such as caking on the dryer walls, product loss, or incomplete drying [5]. Consequently, the main objective of improving the nozzle is to reduce the $x_{90,3}$.

4. Numerical model

The CFD model, including the physics models and the mesh, was implemented in STAR-CCM+ *v*.2206 (Siemens AG, Munich, Germany) as described in our previous work [20]. In short, the multiphase flow that develops in the nozzle was modelled as an immiscible mixture of two phases: The liquid phase was set as incompressible with the Carreau-Yasuda model to represent the non-Newtonian behavior, while the gas phase was assumed as ideal and Newtonian. The implementation Carreau-Yasuda model was validated in our previous work [20], and it was shown that incorporating the non-Newtonian behavior into the simulations did not compromise the accuracy of the simulations.

The multiphase flow was simulated using the Volume-Of-Fluid (VOF) method. This model assumes that all fluid phases share the same pressure and velocity fields. That means that the two-phase system is modelled as a single-phase fluid, whose physical properties are calculated from the volume averages of the properties of the actual phases [26]. In order to resolve the interface between the liquid and the gas, STAR-CCM+ utilizes the High-Resolution Interface Capturing (HRIC) scheme, which is a type of compressive method that ensures that the volume fraction gradient remains sharp near the interface [27]. The validity and accuracy of using a compressive scheme to simulate the multiphase flow inside the ACLR was already evaluated in Ballesteros Martínez and Gaukel [24].

Using the VOF formulation, the internal flow was modelled as transient because of the unstable free surface between the phases. Additionally, to account for turbulence, the Large Eddy Simulation model (LES) was used. With LES, the flow variables are decomposed spatially into a filtered value and a subgrid component [28]. By introducing these decomposed variables into the transport equations, the filtered variables can be resolved directly. In contrast, the subgrid stresses are modelled indirectly, estimating them from the filtered values and a turbulent subgrid viscosity. There are different options to determine the turbulent viscosity. From the recommendations of the user guide [27], the Wall-Adapting Local-Eddy Viscosity (WALE)

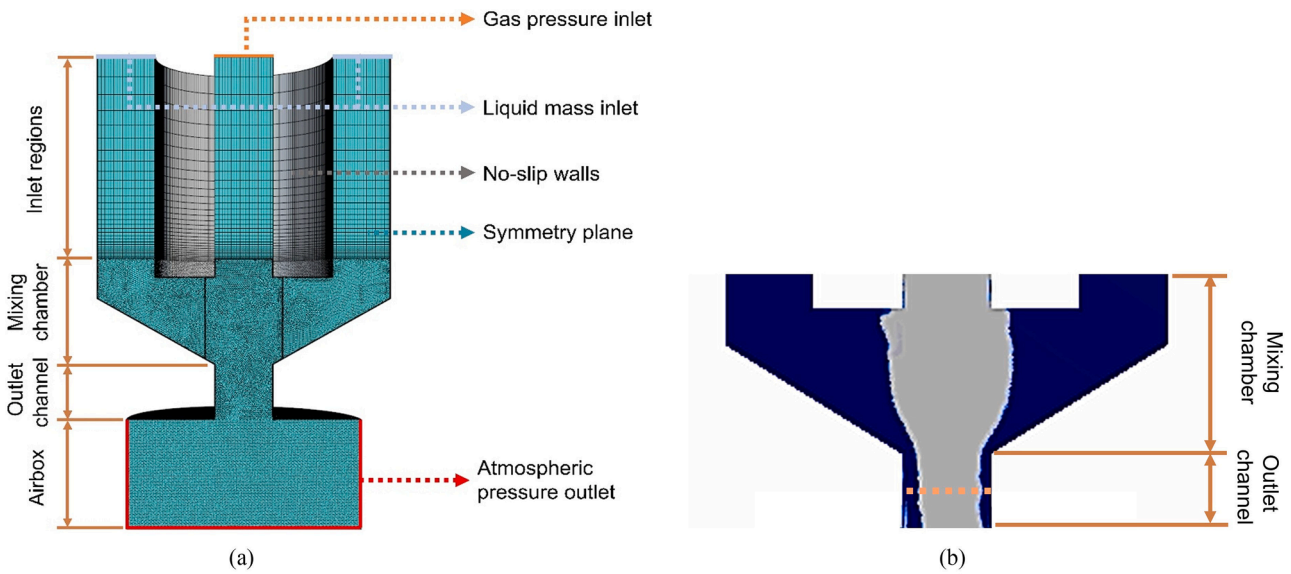

Fig. 2. (a) Simulated mesh of the ACLR atomizer. The boundary conditions are also indicated. Taken from Ballesteros Martinez and Gaukel [33]. (b) 2D snapshot of an exemplary flow pattern inside the mixing chamber and outlet channel of the nozzle. The liquid phase is shown as blue, while the air phase is grey. The dotted orange line is the line probe utilized to measure the liquid lamella thickness.

Table 3
Fitting parameters for the Carreau-Yasuda model for maltodextrin solutions. Taken from Ballesteros Martínez and Gaukel [20].

Dry-matter content [% wt.]	η_0 [Pa·s]	η_∞ [Pa·s]	λ [s]	n [-]	a [-]
52	0.74	0	1.03	0.10	0.38
54	1.33	0	0.49	−0.60	0.46

Table 4
Operating conditions used for the simulations during the geometrical analysis.

Dry-matter content [% wt.]	ALR	Pressure [MPa]	Volume flow [L·h-1]
52	0.19	0.7	25
54	0.17		

Subgrid Scale model was selected [29].

The boundary conditions set for the simulation are shown in Fig. 2a. The gas pressure and the liquid flowrate were the inlet boundary conditions set in the simulations. The exit of the simulated volume was set as an atmospheric pressure outlet. Because only half the nozzle was simulated, a symmetry plane was implemented. All simulations were run for at least 8 ms. We accounted for 4 ms of initialization time and 4 ms for the time-dependent and time-averaged analysis. An adaptive timestep was introduced to ensure the stability of the solver, and it usually stabilized around 50 ns.

The mesh configuration and density was based on the mesh independence analysis done on our previous study, which was performed for a quarter of a nozzle [24]. The regions of interest, i.e. the mixing chamber and the outlet channel, were meshed with a fine polyhedral grid. Conversely, the inlet regions upstream, where there is exclusively either gas or liquid, were fitted with a coarser hexahedral grid. The adequacy of the mesh was determined using the Kolmogorov and Taylor length scales, which are good criteria for the minimum and maximum local cell sizes, respectively, that an appropriate mesh should have. More details about this analysis can be found in Ballesteros Martínez, Becerra, and Gaukel [30]. The chosen mesh has a reference cell size of 33 mm, a cell count of 1.3 million cells, and it can be seen in Fig. 2a.

To characterize the internal flow instabilities, that is the fluctuations of the annular flow, we utilized the lamella thickness (h). For this purpose, a linear probe was created in the middle of the outlet channel, with the same length as the channel radius. The exact position of the probe is shown in Fig. 2b, along with an exemplary snapshot of the annular flow that forms inside the nozzle. Following the method established by Ballesteros Martínez and Gaukel [24], the liquid volume fraction was measured along the line. Then, using a line integral, we calculated the portion of the line probe occupied by the liquid phase. This calculation of the lamella thickness was performed at each timestep during the 4 ms of simulation that were used for analysis. To characterize the lamella thickness fluctuations along this time, the 5 %, 50 %, and 95 % percentiles were calculated and are denoted as $h_{5,0}$, $h_{50,0}$, and $h_{95,0}$, respectively. Because a thicker lamella is correlated with larger droplets [18], the geometrical analysis and optimization of the nozzle design are biased toward primarily reducing the $h_{95,0}$.

5. Operating conditions

To compare all the geometrical variations of the nozzle, it was important to use the same conditions, and to choose a condition that is representative for the desired application with the ACLR nozzle and the atomization of highly viscous feeds. Therefore, all simulations were carried out using the properties of a 52 % wt. maltodextrin solution. Additionally, once the improved nozzle design was generated, it was also tested with a higher dry-matter mass fraction, of 54 % wt., to ensure that the improvement of the internal flow stability was not restricted to a specific viscosity. The rheology of maltodextrin solutions at this range of dry-matter concentrations has been shown to be strongly shear-thinning, so the non-Newtonian Carreau-Yasuda model [31,32] was used to represent this behavior. The equation of the model is:

$$\eta(\dot{\gamma}) = \eta_\infty + (\eta_0 - \eta_\infty)(1 + (\lambda \cdot \dot{\gamma})^a)^{(n-1)/a} \quad (1)$$

where η is the viscosity, η_0 is the zero viscosity, η_∞, the viscosity at infinite shear rate, and $\dot{\gamma}$ is the shear rate. The correlation parameters are the relaxation time λ, the power index n, and the parameter a, which controls the shear-thinning behavior. Table 3 shows the model parameters that represent the behavior of the solutions at the different maltodextrin concentrations.

Similarly, all simulations were carried out under the same pressure and volume flow, which are summarized in Table 4. The resulting ALR

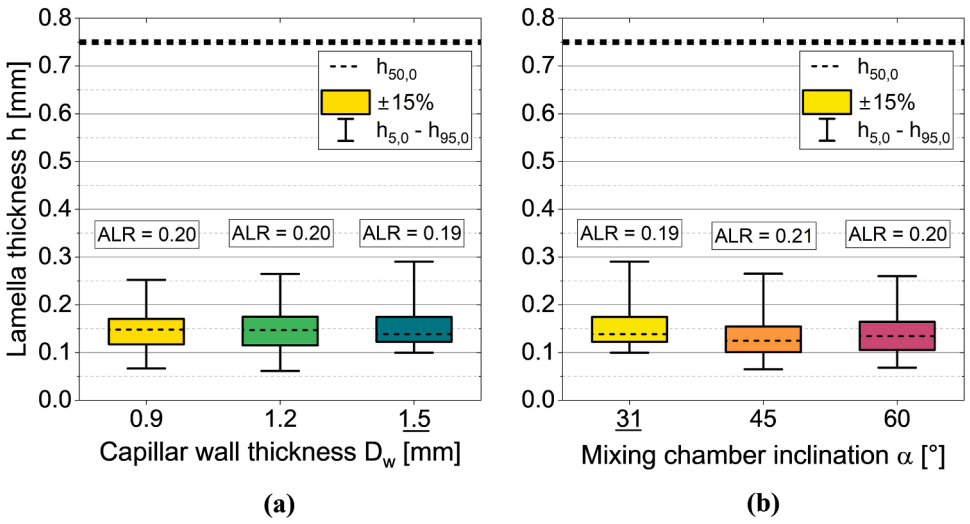

Fig. 3. Box diagram of lamella thickness for the 52 % wt. MD solution at 0.7 MPa and a liquid volume flow of 25 L/h, for different values of the: (a) capillary wall thickness and (b) mixing chamber inclination. The underlined value in the x-axis marks the dimension of the base geometry. The box width correlates to $a \pm 15$ % interval around the median. The whiskers mark the 95 % and 5 % percentiles. The resulting median ALR is also indicated. The dotted line represents the maximum thickness that the lamella can reach.

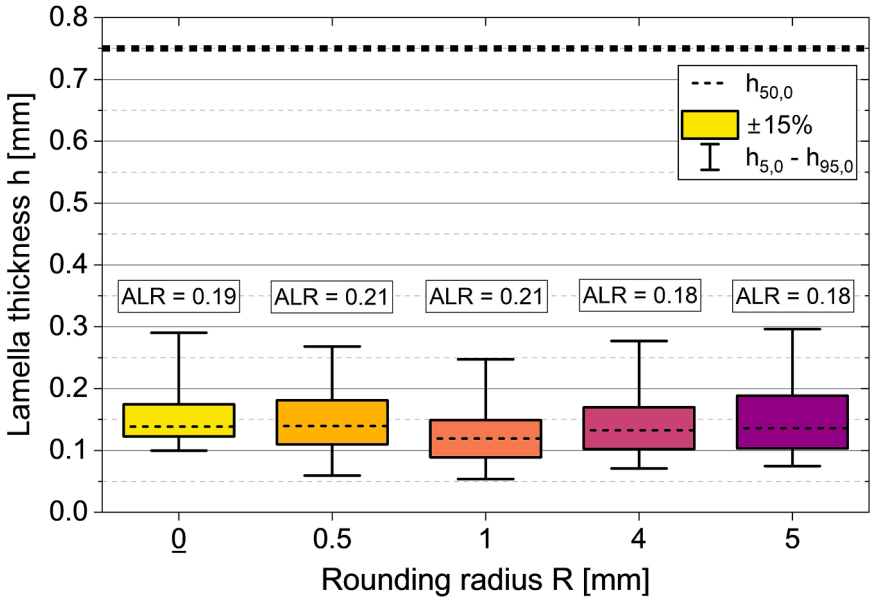

Fig. 4. Box diagram of lamella thickness for the 52 % wt. MD solution at 0.7 MPa and a liquid volume flow of 25 L/h, for different rounding radii. The underlined value in the x-axis marks the dimension of the base geometry. The box width correlates to $a \pm 15$ % interval around the median. The whiskers mark the 95 % and 5 % percentiles. The resulting median ALR is also indicated. The dotted line represents the maximum thickness that the lamella can reach.

from the base geometry is also indicated for each maltodextrin solution. As it will be discussed in Section 6.4, the geometrical variations have an effect on the ALR. In turn, the ALR also has an effect on the flow instabilities. To differentiate between the direct effect of the geometrical parameters and the effect of a higher/lower ALR, some of the simulations were repeated with a specified ALR instead of a set pressure. It should be noted, however, that the ALR could not be directly set in the simulations, because the boundary conditions of the CFD model are the inlet pressure of the gas and the volume flow of the liquid. These are also the parameters that can be adjusted in the experimental spray rig. It is not possible to simultaneously set the mass flow and the pressure of the gas, as that would overspecify the boundary condition [27]. To circumvent that, we implemented a target mass flow in the pressure inlet boundary, which allows the program to change the inlet gas pressure (from an initial user-defined value) between iterations until the desired air mass flow is reached. More details about how the implementation of the gas inlet conditions affects the simulation are discussed in Appendix B.

6. Results and discussion

Sections 6.1–6.3 detail the results from the geometrical variations of the base nozzle geometry. The different parameters are grouped according to which nozzle section was altered. Section 6.4 focuses on the effect that the geometrical variation has on the ALR and how this affects the flow stability. Section 6.5 consists of the evaluation of the improved nozzle design.

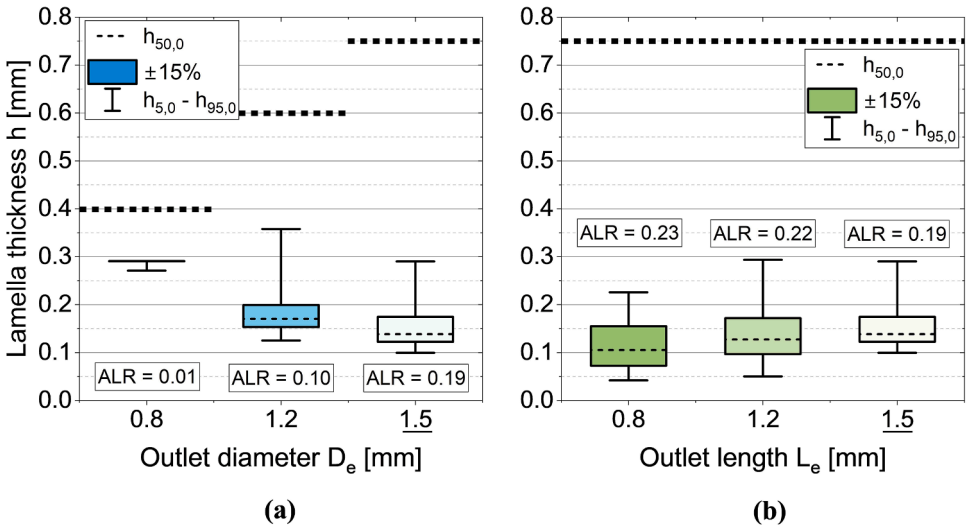

Fig. 5. Box diagram of lamella thickness for the 52 % wt. MD solution at 0.7 MPa and a liquid volume flow of 25 L/h, for different values of the: (a) outlet diameter; and (b) outlet length. The underlined value in the x-axis marks the dimension of the base geometry. The box width correlates to $a \pm 15$ % interval around the median. The whiskers mark the 95 % and 5 % percentiles. The resulting median ALR is also indicated. The dotted line represents the maximum thickness that the lamella can reach.

6.1. *Effect of the mixing chamber dimensions ($\mathbf{D_w}$, $\boldsymbol{\alpha}$) on flow stability*

Fig. 3 shows the time-dependent variations of the lamella thickness, as a box diagram, for different α and D_w. As a general comment, all median values are in the range of 0.12–0.15 mm. The main effect of the geometrical variations is seen on the shift of the $h_{5,0}$ and $h_{95,0}$ values.

Looking specifically at the capillary wall thickness, Fig. 3a shows that the value range of the distribution tends to increase with increasing wall thickness, which is illustrated by the 5 %–95 % whiskers. In contrast, the median and its surrounding range of ±15 % remain almost constant, showing only a small decrease of around 7 % with the largest D_w. From this, it can be concluded that thinner capillary walls cause the lamella fluctuations to decrease but the median lamella to increase. The ALR, on the other hand, only decreases marginally with thicker capillary walls. Considering these results, decreasing the capillary wall thickness has contrary effects on the $h_{95,0}$ (decreasing) and the median (increasing), so it might not be the most recommendable option to change for the improved design.

For the chamber inclination (Fig. 3b), there is a decrease in the lamella fluctuations, when comparing 31° to the other two angles, which would agree with the expectations explained in Table 1. The median lamella thickness is reduced by around 10 % when increasing the chamber inclination to 45°. However, the median then increases again (although <5 %) when the inclination changes from 45° to 60° The reason for this is not clear. The results from the simulations show that the average shear rate of gas on the liquid surface increases from 2.7×10^5 to 2.9×10^5 s^{-1}, when the chamber inclination increases from 31° to 45°. It then decreases to 2.6×10^5 s^{-1}, when the inclination is increased to 60°. Therefore, there might be an optimal impingement angle between the phases that minimizes the change of flow direction but maximizes the transfer of energy of the gas into the liquid. At least from the values analyzed, 45° would be the most adequate option. With regards to the ALR, there is a small increase of <10 % as the inclination angle becomes larger. However, it should be noted that the increase is minimal compared to the normal fluctuation of the ALR (see Appendix B).

6.2. *Effect of the rounded corners (**R**) on flow stability*

Fig. 4 shows a box plot of the lamella thickness for different rounding radii. In general, all percentiles decrease with larger R to a minimum at around 1 mm and then begin to increase again. In fact, a radius of 5 mm leads to a wider range of variation (difference between the $h_{5,0}$ and the $h_{95,0}$) compared to no edge rounding at all. This might be related to the lower ALRs that occur at 4 and 5 mm. Conversely, smaller rounding radii favor higher ALRs, under the same pressure conditions. It may also be, that the nozzle becomes too round with the higher radii, and it can no longer induce the formation of a stable annular flow. In the range of values tested, rounding off the edges with a radius of 1 mm seems to be the optimum to reduce the lamella thickness values and its range of variation, as it presents the lowest $h_{50,0}$ and $h_{95,0}$.

6.3. *Effect of the outlet channel dimensions ($\mathbf{L_e}$, $\mathbf{D_e}$) on flow stability*

Fig. 5 shows the effects of the dimensions of the nozzle outlet channel on the lamella thickness, more specifically of the outlet diameter (in Fig. 5a) and length (in Fig. 5b). As in Fig. 4, a box plot diagram is used to illustrate the statistical distribution of the measured values. Starting with the D_e, it is evident that the outlet diameter has a decisive effect on the resulting lamella thickness. However, contrary to what was hypothesized in Table 1, a smaller diameter leads to a thicker liquid lamella, as it can be seen when comparing 1.2 and 1.5 mm. When reducing further to 0.8 mm, the flow is almost choked, and a very thick lamella, almost as thick as the entire radius of the outlet (0.4 mm for that geometry), forms. Additionally, the thick lamella presents very little variation. That is why the box diagram seems to collapse into a line. The reason for this behavior may lie in the strong reduction of the ALR, when the diameter is reduced at a constant pressure. The rise in lamella thickness with decreasing D_e does not agree with the results of Wittner et al. [23] and Hammad et al. [7]. However, their work was restricted to much lower viscosities lower than 0.12 Pas. It may be that the pressure losses when operating with higher viscosities, like in this work, outweighs any benefits from the larger gas velocity that come from the reduced diameter.

On the other hand, when looking at the results of the outlet length (Fig. 5b), the median of the lamella thickness increases consistently with a longer outlet channel. The 5 % and 95 % percentiles also increase, though at an inconsistent rate. $h_{5,0}$ increases most from 1.2 to 1.5 mm, while the $h_{95,0}$ increases most from 0.8 to 1.2 mm. This causes the range of variation to be actually the largest for 1.2 mm. Nonetheless, the fact that a shorter outlet channel leads to a more stable and thinner lamella with what Schröder et al. [22] observed for a similar internal-mixing

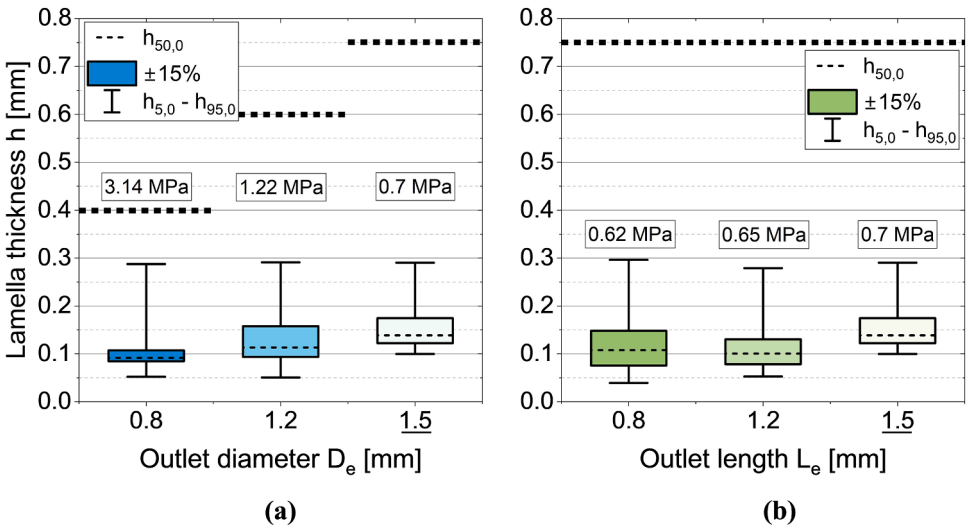

Fig. 6. Box diagram of lamella thickness for the 52 % wt. MD solution at a target ALR of 0.19 and a liquid volume flow of 25 L/h, for different values of the: (a) outlet diameter; and (b) outlet length. The underlined value in the x-axis marks the dimension of the base geometry. The box width correlates to $a \pm 15$ % interval around the median. The whiskers mark the 95 % and 5 % percentiles. The resulting average inlet pressure is also indicated. The dotted lines represent the maximum thickness that the lamella can reach.

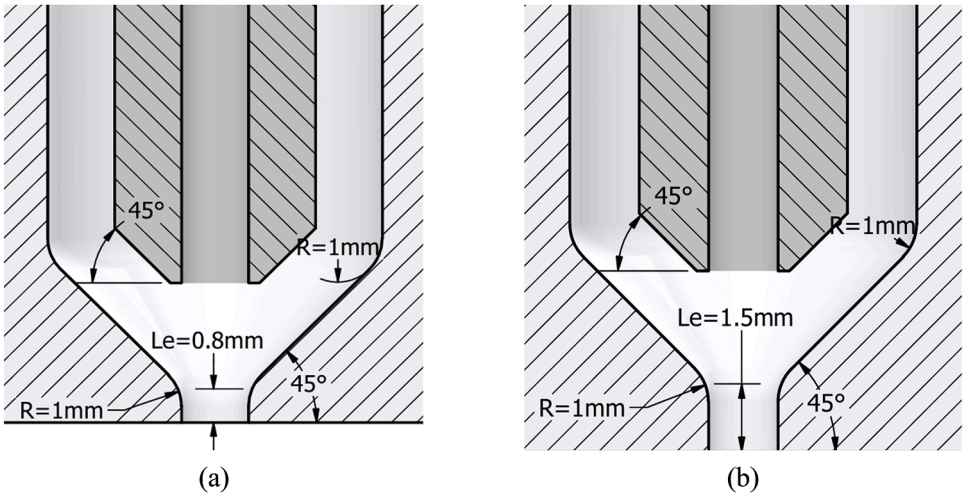

Fig. 7. Schematic of the proposed improved nozzle geometries: (a) improved nozzle 1 with $\boldsymbol{L_e} = 0.8$ mm; and (b) improved nozzle 2 with $\boldsymbol{L_e} = 1.5$ mm.

nozzle, the effervescent atomizer. Shortening the contact time between the phases, by reducing L_e or L_m, leads to a more stable lamella thickness. On top of that, the shortened outlet channel also allows a higher ALR under constant operating pressure, which has also a positive effect in reducing the lamella fluctuations. It is clear then that an improved nozzle should have a shorter outlet length.

6.4. Separating effects of geometric parameters from the ALR

As noticed in Sections 6.1–6.3, varying the nozzle dimensions has both an effect on the lamella thickness and on the ALR, which, in turn, has an effect on the lamella thickness. Therefore, it was of interest to distinguish between a direct influence of the geometrical parameters on the flow instabilities and a secondary effect from the higher/lower ALRs. For this purpose, we implemented alternate boundary conditions, as explained in Section 5, in a way that the same ALR was reached in the new geometry as in the base geometry. We conducted this analysis for the geometrical parameters that showed the largest ALR deviations: the outlet diameter and outlet length.

The results are shown in Fig. 6, which presents the fluctuations in lamella thickness over time at a constant ALR of 0.19. The box plot diagram is analogous to the diagram at a constant pressure of 0.7 MPa (see Fig. 5). When operating at the same ALR, it is clear that both smaller outlet lengths and diameters lead to thinner lamellas, with a strong reduction of the $h_{50,0}$. This agrees with what was expected from Table 1. The effect on the $h_{95,0}$ is not as clear. However, one important thing to notice is the average pressure required to achieve the ALR of 0.19. For the L_e, there is little difference between the pressures. However, for the D_e, the pressure increases over 400 %, when the diameter is reduced to from 1.5 to 0.8 mm. This confirms our previous conclusions that the improved nozzle should have a shorter outlet length but the base diameter.

6.5. Improved nozzle design

Based on the knowledge gained from Sections 6.1–6.4, it becomes clear that an improved nozzle would need to have a shorter L_e, a larger α, and its internal edges rounded off. Determining the specific optimal value for each of these parameters would have required a much more extensive simulation plan, so instead we combined the simulated

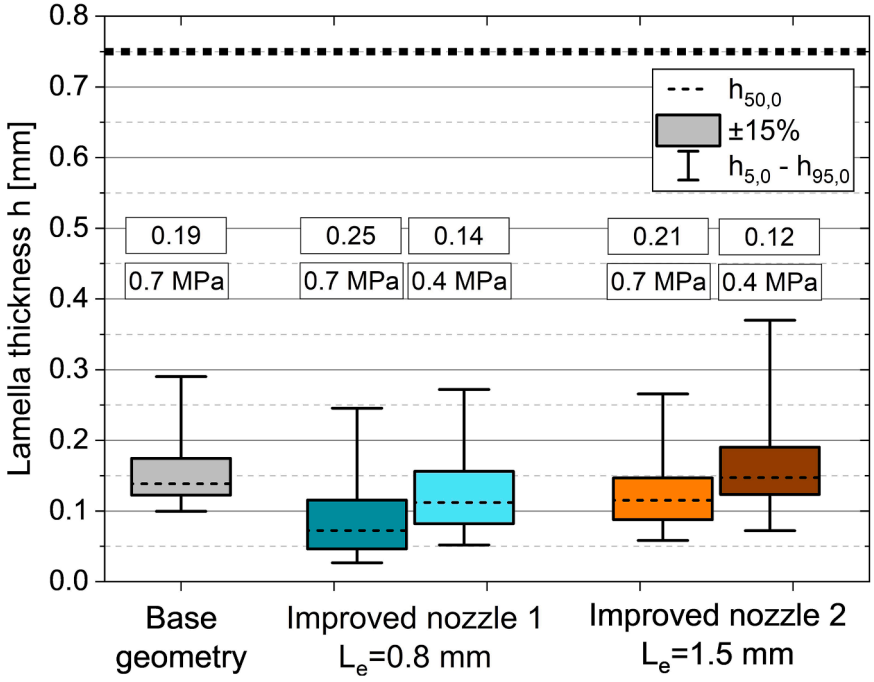

Fig. 8. Box diagram of lamella thickness for the 52 % wt. MD solution at 0.4 and 0.7 MPa and a liquid volume flow of 25 L/h, for the base geometry and the two proposed improved nozzle designs. The box width correlates to $a \pm 15$ % interval around the median. The whiskers mark the 95 % and 5 % percentiles. The dotted line represents the maximum thickness that the lamella can reach. The corresponding pressure and ALR are noted on top of each measurement.

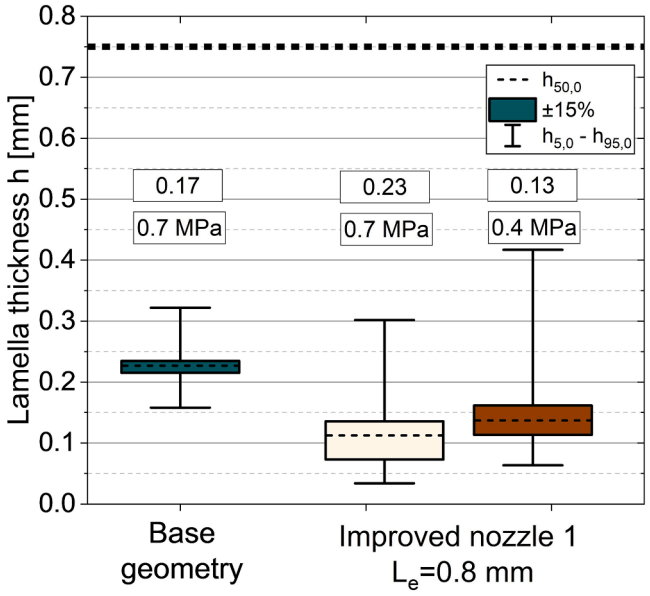

Fig. 9. Box diagram of lamella thickness for the 54 % wt. MD solution at 0.4 and 0.7 MPa liquid volume flow of 25 L/h, for the base geometry and the improved nozzle design. The box width correlates to $a \pm 15$ % interval around the median. The whiskers mark the 95 % and 5 % percentiles. The dotted line represents the maximum thickness that the lamella can reach. The corresponding pressure and ALR are noted on top of each measurement.

dimensions that provided the best results. This leads to the improved nozzle 1 shown in Fig. 7a. The effect of the D_w was not as clear, given that the median lamella thickness increased while the $h_{95,0}$ decreased, so we considered it best to maintain the original value. Additionally, a thicker capillary wall allows additional safety when handling larger pressures and makes construction of the nozzle easier. The original D_e was also maintained, because decreasing it raises the pressure requirements of the nozzle (see Fig. 6a) and increasing it leads to a higher SMD [23].

In general, we expected that the different geometrical variations would not negatively interact with each other when combined, as they all should lead to thinner and more stable lamellas. The single exception was that rounding off the edges with an R of 1 mm plus having a shorter L_e might not allow enough length for the annular flow to develop. To evaluate if this is a valid concern, we also included an alternative improved nozzle 2, with an L_e of 1.5 mm, which is shown in Fig. 7b.

With that in mind, the internal flow stability of the optimized nozzles was examined. The box plot diagram of the two improved designs is shown in Fig. 8. Comparing the simulations at 0.7 MPa, it is clear that the geometrical changes lead to reduced lamella thicknesses, with both the median and the $h_{95,0}$ being smaller than those of the base geometry. The greatest improvement can be seen in the shorter L_e. Consequently, there seems to be still enough length for the annular flow to develop. An even more interesting finding is that, when simulating the same geometries at 0.4 MPa, the improved nozzle 1 still presents thinner lamellas than the base geometry, with an $h_{50,0}$ around 20 % smaller. This could mean that the improved design could operate at a lower pressure and still obtain smaller or similar lamella thicknesses than the base geometry, which could lead to smaller operating costs in industrial applications. In contrast, the improved nozzle 2, with L_e of 1.5 mm, shows larger lamella variations than the base geometry when operating at a lower pressure, which is the expected result. Overall, it can be seen that the improved design 1 is the most promising one.

It is possible that the apparent reduced pressure requirements of the improved nozzle 1 are simply due to larger ALRs, which is why the ALRs were determined as shown also in Fig. 8. As expected, when operating at the same pressure, the improved nozzles present a larger ALR than the base geometry. However, contrary to the initial expectation, the ALR of the improved nozzle 1 at 0.4 MPa is smaller than the one of the base geometry at 0.7 MPa, even though it has a thinner lamella with smaller fluctuations. This outcome highlights that the geometrical improvement leads to a more stable and smaller lamella thickness. In addition, the smaller pressure and ALR requirements could even further lower energy

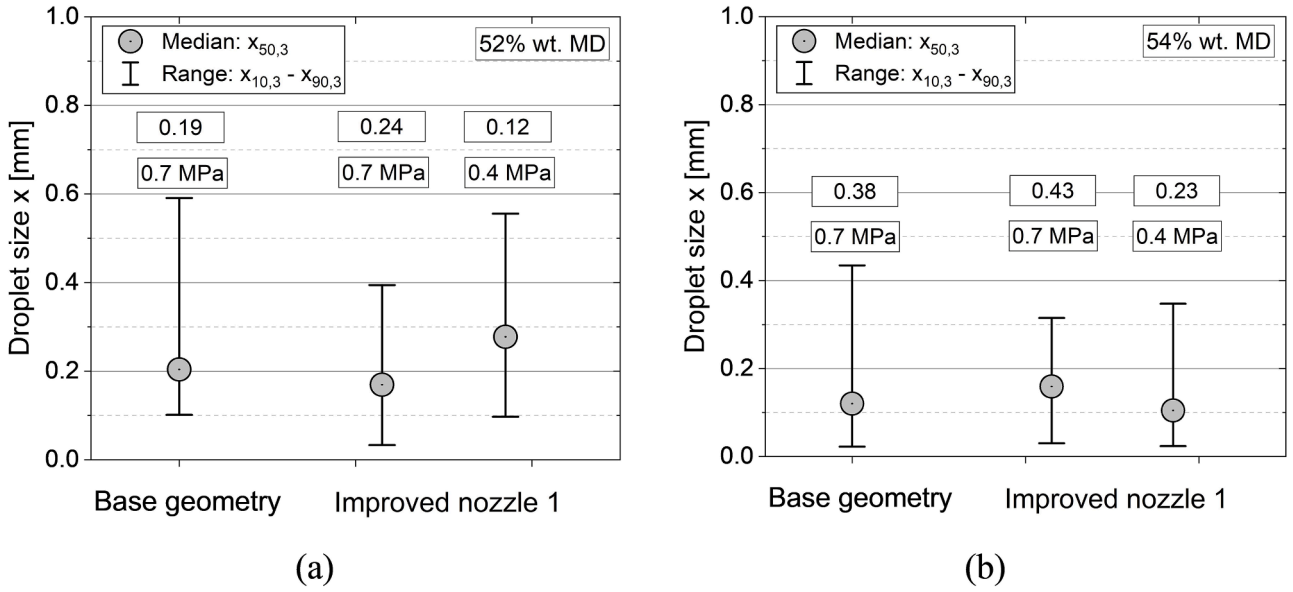

Fig. 10. Median and range of the experimental droplet size distributions, at 0.4 and 0.7 MPa, for the base geometry and the improved nozzle designs for: (a) 52 % wt. MD solution with a liquid volume flow (Q_L) of 25 L/h; and (b) 54 % wt. MD solutions with a Q_L of 15 L/h. The pressure and the corresponding ALR are noted on top of each distribution.

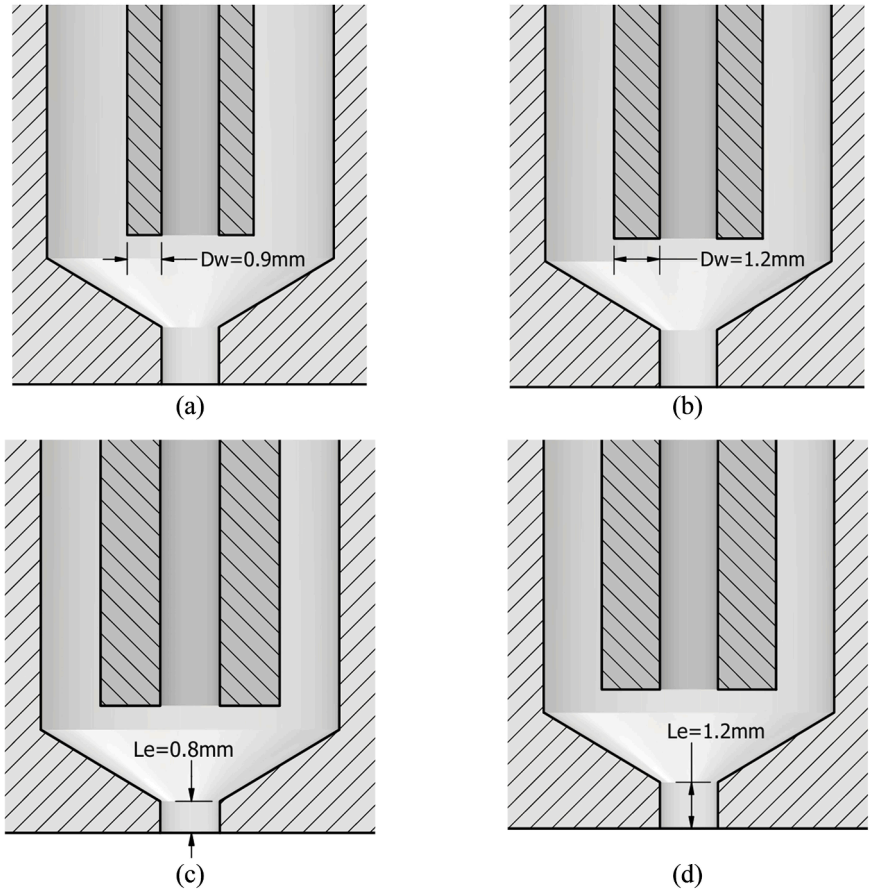

Fig. 11. Schematic of the nozzle geometry with all base parameters except for: (a–b) the wall thickness (D_w) of the gas capillary; and (c–d) the length (L_e) of the outlet channel. In the case of the D_w, it was decreased from its original 1.5 mm to (a) 0.9 mm; and (b) 1.2 mm. In the case of L_e, it was decreased from its original 1.5 mm to (c) 0.8 mm; and (d) 1.2 mm.

consumption and operating costs.

To further evaluate the applicability of the improved nozzle 1, we investigated its operation with a higher viscosity of 1.33 Pa·s, which corresponds to a maltodextrin solution of 54 % wt. The resulting lamella thicknesses are plotted in Fig. 9, both for the improved nozzle and the base geometry. Just as it was observed for the lower viscosity, the

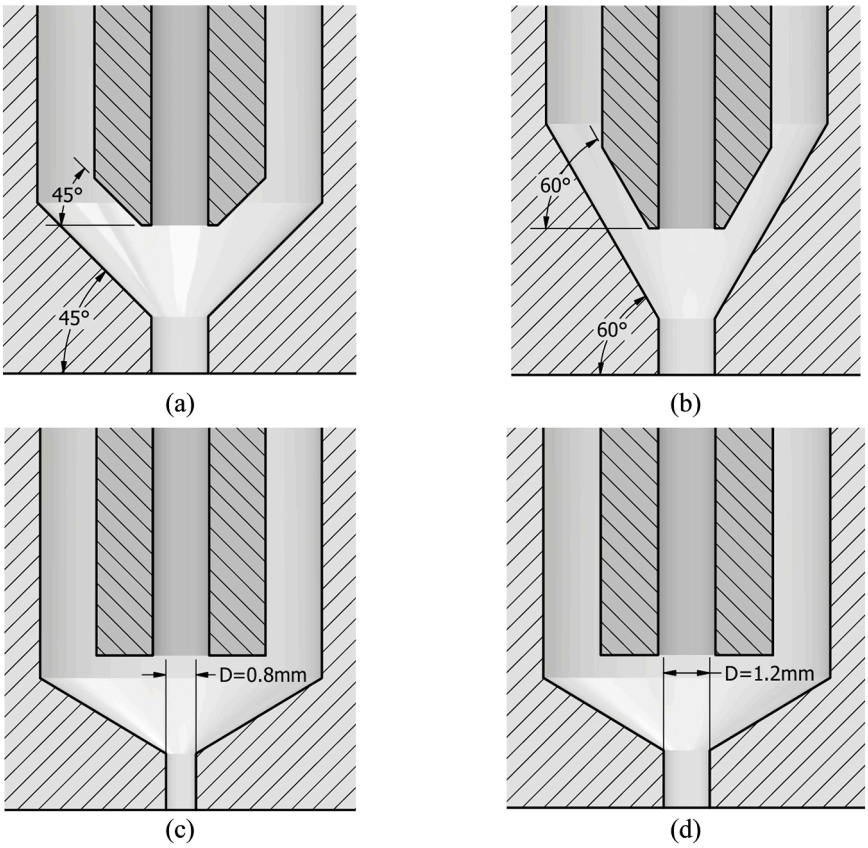

Fig. 12. Schematic of the nozzle geometry with all base parameters except for: (a–b) the inclination (α) of the mixing chamber; and (c–d) the diameter (D_e) of the outlet channel. In the case of the α, it was increased from its original 31° to (a) 45°; and (b) 60°. In the case of D_e, it was decreased from its original 1.5 mm to (c) 0.8 mm; and (d) 1.2 mm.

improved design shows much smaller values for the lamella thickness, compared to the base design, when operating at the same pressure, mostly because the resulting ALR is larger (also shown in the figure). However, in this case, lowering the pressure to 0.4 MPa leads to a wider range of variation compared to the base design at 0.7 MPa. Taking into account that the viscosity in this case is about double of that in Fig. 8, it was to be expected that the performance at 0.4 MPa would be worse. Nonetheless, it should be kept in mind that even operating at 0.7 MPa, the improved geometry still requires far lower ALRs than commercial external-mixing nozzles, which normally require ALRs of 1–15 [14].

6.6. Experimental evaluation of the improved nozzle design

As a final proof of concept, we compared the actual performance of the improved nozzle with the base design, on a spray test rig. For this purpose, the improved nozzle 1 was manufactured as two pieces: a metal capillary tube for the gas and a clear acrylic block around it, which receives the liquid feed. The most important parameter to evaluate is the DSD, since the resulting droplet sizes have a large influence on the drying kinetics as well as on the properties of the final powder. Fig. 10 shows how the droplet sizes compare between the designs, for two different MD concentrations. Following the same logic as in Section 6.5, we not only compared the two designs using the same inlet pressure, but also evaluated a lower pressure with the improved geometry, to highlight the lower pressure requirements of the improved design.

The data shows that the improved nozzle generates smaller $x_{90,3}$ compared to the base design. This holds true even when operating the improved nozzle at a lower pressure, and it occurs with both evaluated solutions. The effect of the geometry on the median droplet sizes is not as clear. For 52 % wt., it follows a similar trend as the $x_{90,3}$, decreasing when $x_{90,3}$ decreases. However, for 54 % wt., the median is actually at its highest when the $x_{90,3}$ is at its lowest. As for the $x_{10,3}$, it becomes smaller with the improved nozzle, for 52 % wt., but it shows almost no change when atomizing the 54 % wt. solution. Overall, given that the $x_{90,3}$ is a critical factor for the operability of an spray dryer [5], it is an important finding that the geometry improvement has such a positive effect on reducing the $x_{90,3}$.

It might jump to the attention of the reader that the droplet sizes are lower for the MD solution with a higher viscosity, which seems counter intuitive. The reason for this difference is that, in the experimental setup, the maximum volume flow that could be achieved decreased for higher viscosities [12]. This means that each solution was evaluated at a different volume flow and, therefore, at a different range of ALRs (this is also noted in Fig. 10). Nonetheless, the difference in ALR range had no real effect on the geometry analysis. It simply means that the performance with the different feed viscosities cannot be compared directly with each other.

Similar to the previous analysis of the lamella thicknesses, it is important to verify if the positive effect of the improved geometry on the droplet sizes are simply caused by larger ALRs. For that purpose, we compare the ALRs and droplet sizes shown in Fig. 10. As expected, when operating at the same pressure, the improved nozzle presents both a higher ALR and smaller droplets ($x_{90,3}$) than the base design. However, we can also see that when we reduce the operating pressure to 0.4 MPa, the improved nozzle still maintains an $x_{90,3}$ smaller than that of the base geometry at 0.7 MPa, even though its ALR at 0.4 MPa is lower than the one of the base design. This holds true for both viscosities, and it confirms the lower operating requirements of the improved nozzle design, which would also mean lower operating costs.

An important disclaimer to address here is that, although the improved nozzle presents a smaller $x_{90,3}$ than the base design, the value is still higher than what is recommended for most industrial

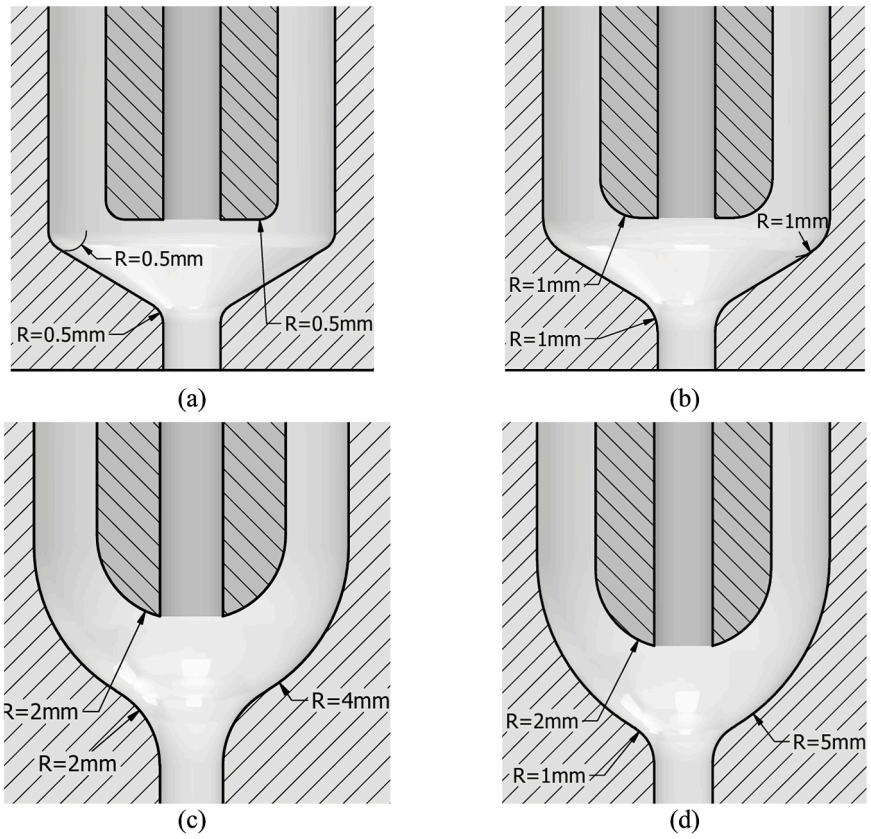

Fig. 13. Schematic of the nozzle geometry with all base parameters except for the rounded internal edge. Different nominal rounding radii were evaluated: (a) 0.5 mm; (b) 1.0 mm; (c) 4 mm; and (d) 5 mm.

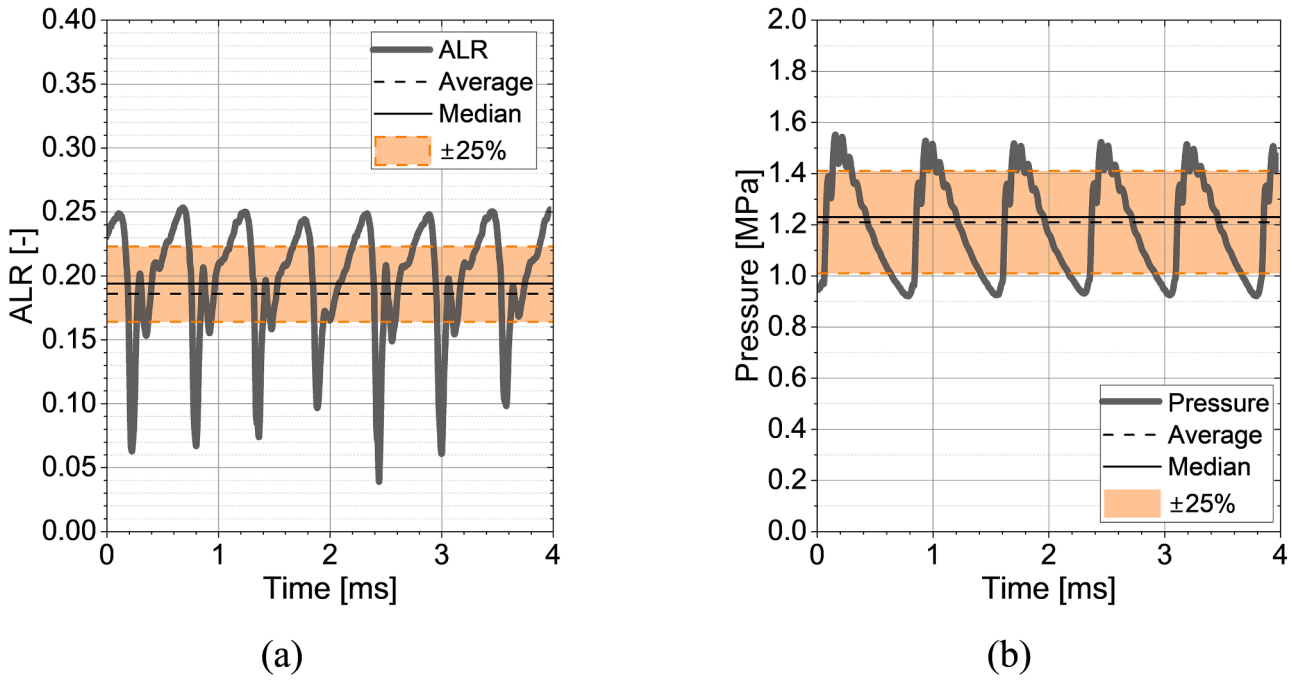

Fig. 14. Example of time-dependent profile, as well as the average, the median, and the ±25 %-range of variation around the median, for: (a) the ALR of a simulation with a fixed inlet pressure of 0.7 MPa and a liquid volume flow of 25 L/h, with the basic geometry; and (b) the inlet pressure for a simulation with a specified target ALR of 0.19 and a liquid volume flow of 25 L/h, with a modified geometry with $D_e = 1.2$ mm.

applications. As a reference, for the spray drying of milk products, coffee, pigments and even ceramics, the expected droplet sizes should not exceed 200–400 µm [5]. Nonetheless, it should be noted that the ALRs are very low compared to those of commercially available pneumatic

nozzles, such as air-blast nozzles, which usually require ALRs between 1 and 15 [14]. Therefore, increasing the atomization pressure could be considered to further reduce the $x_{90,3}$, if the experimental setup allows it. The simulation results from Ballesteros Martínez and Gaukel [20] show that the maximum lamella thickness can be strongly reduced while remaining at ALRs below 1. This would indicate that further reduction of the $x_{90,3}$ should also be possible while maintaining the benefit of low ALR requirement that the ACLR nozzle has with respect to other pneumatic nozzles. Because the vast majority of the energy consumption in the spray-drying process occurs during the drying step (over 95 % [3]), increasing the ALR would not significantly reduce the potential 45 % energy savings achieved by implementing the ACLR in a standard process.

7. Conclusions

The geometrical design of the ACLR was investigated and improved using a validated CFD model. Six parameters were considered: the diameter and wall thickness of the gas capillary, the length and inclination of the mixing chamber, and the length and diameter of the outlet channel. Additionally, we considered the possibility of rounding off the sharp corners of the nozzle with different radii. The influence of these parameters on the internal multiphase flow was analyzed, with the intent on minimizing the thickness of the liquid lamella that forms inside the nozzle. The results showed that a shorter outlet length, a larger chamber inclination, and rounded internal edges produced thinner and more stable liquid lamellas.

Based on these findings, two optimized designs were proposed, differing only in outlet length (0.8 and 1.5 mm). The purpose of evaluating two outlet lengths was to verify whether combining the rounded internal edges with a shorter outlet channel could hinder the development of the internal flow. This, however, was not the case, as simulations indicated that the shorter outlet (0.8 mm) generated thinner and more stable lamellas. Based on this result, this version of optimized nozzle was manufactured and tested in an experimental spray rig, by comparing its droplet size distribution with that of the base design. The optimized nozzle consistently produced smaller droplet sizes and generally performed better than the base design, even at lower pressures and ALRs. This outcome highlights that the geometrical improvement leads to a more stable and smaller lamella. Not only that, but the smaller pressure and ALR requirements could even further lower energy consumption and operating costs.

Statements and declarations

This work was partly funded by the Deutsche Akademische Austauschdienst (DAAD), through one of their research grants for doctoral programs in Germany. The authors also acknowledge the financial support of the International Fine Particle Research Institute (IFPRI). The authors do not have any competing interests to declare that are relevant to the content of this article.

CRediT authorship contribution statement

Miguel Ángel Ballesteros Martínez: Writing – review & editing, Writing – original draft, Validation, Software, Methodology, Investigation, Funding acquisition, Formal analysis, Data curation, Conceptualization. **Benedikt Heider:** Writing – review & editing, Visualization, Software, Investigation, Formal analysis, Data curation. **Volker Gaukel:** Writing – review & editing, Supervision, Project administration, Funding acquisition, Conceptualization.

Declaration of competing interest

The authors declare the following financial interests/personal relationships which may be considered as potential competing interests:

Miguel Ángel Ballesteros Martínez reports financial support was provided by German Academic Exchange Service. Volker Gaukel reports financial support was provided by International Fine Particle Research Institute. If there are other authors, they declare that they have no known competing financial interests or personal relationships that could have appeared to influence the work reported in this paper.

Acknowledgments

The authors would like to thank Markus Fischer and Jürgen Kraft for their assistance in manufacturing the improved nozzle design and ensuring the correct functioning of the experimental setup.

Appendix A. Geometrical variations of the ACLR nozzle

The geometrical analysis was conducted with the principle of varying only one specific parameter while keeping all the rest constant. In some cases, this could be done directly, like the alternative geometries shown in Fig. 11 for the D_w and the L_e.

Varying a single parameter without altering anything else in the nozzle was, however, not always possible. In the case of the variations of α, keeping all other nozzle dimensions the same meant chamfering the outer edge of gas capillary. This is shown in the alternative geometries of Fig. 12a–b. By chamfering the gas capillary, the L_m can be maintained without the gas capillary and the outer casing colliding with each other. One point to notice, especially in Fig. 12b, is that increasing the inclination angle of the mixing chamber decreases the cross-sectional area available for the liquid flow. This, however, cannot be avoided without also having to alter the L_m by changing the position of the gas capillary. Therefore, it was simply considered a secondary effect of changing α.

Similarly, changing the outlet diameter D_e could not be done without altering the L_m, is it can be seen in Fig. 12c–d. Trying to maintain the same L_m would have meant changing the α or moving the gas capillary, so we considered the change in L_m as simply a secondary effect of varying the outlet diameter. The effect was also minor. The L_m in Fig. 12c changed from 2.4 mm to 2.61 mm; for Fig. 12d, it changed to 2.49 mm.

Finally, Fig. 13 shows how the different rounding radii were implemented into the nozzle. As it can be noticed, the large radii (4 and 5 mm) could not be implemented in all the edges, mainly because of spatial restrictions. In those cases, the edge was rounded off to the largest radius that was physically possible. For simplicity, only integer values were considered.

Appendix B. Setting the air inlet conditions and its effect on the simulation

The inlet boundary of the air phase in the simulation allows one to either set a fixed pressure or a fixed mass flow, but not both at the same time. Moreover, setting the inlet pressure (which is the boundary configuration used in all these simulations) leads to a fluctuation of the ALR across time, as it can be seen in Fig. 14a. Looking at the asymmetrical fluctuations in Fig. 14a, the median value might be more useful, and it is the value used in this study, when comparing simulations. For simplicity, the median value of the ALR is simply denoted as ALR, instead of $ALR_{50,0}$.

With regards to the causes for these fluctuations in the ALR, they are most likely the result of the compressibility of the gas and the small volume of

gas that is being simulated. In comparison, the volume of gas in a normal experimental setup is much larger, so it can buffer the local variations in the gas pressure and density. Nonetheless, over 50 % of the measured values fall within ±0.03 of the median, so the small fluctuations and the short-lived large peaks are not considered to be an important source of error for the simulations.

That is why we implemented a target mass flow in the pressure inlet boundary, for the simulations where we were comparing the nozzles at a constant ALR. This means that, while the boundary is still a pressure inlet, the program adjusts the set inlet pressure every 50 timesteps so that the specified mass flow is reached and maintained [27]. This correction leads to a fluctuation in the inlet pressure, as shown in Fig. 14b. Nonetheless, the fluctuation is symmetrical around the average value, so the average can be used to compare the inlet pressures between geometrical variations, as it can be seen in Section 6.4.

Data availability

Data will be made available on request.

References

[1] European Commission. Directorate General for Energy, B.V. Trinomics, Oeko. Enerdata, E3M., Ludwig Bölkow SystemTechnik., Study on Energy Prices and costs: Evaluating Impacts On Households and industry: 2023 Edition, Publications Office, LU, 2024. https://data.europa.eu/doi/10.2833/782494. accessed November 26, 2024.

[2] I.C. Claussen, S. Sannan, M. Bantle, M. Lauermann, V. Wilk, Specification of Performance Indicators and Validation requirements, EU Project No.: 723576 “DryFiciency Waste Heat Recovery in Industrial Drying Processes”, European Union, 2021. https://dryficiency.eu/wp-content/uploads/2021/08/D1_2_Performance-indicators-and-validation-requirements_Update-Scanship.pdf. accessed March 4, 2024.

[3] M. Fox, C. Akkerman, H. Straatsma, P. Jong, Energy reduction by high dry matter concentration and drying, New Food 6 (2010) 60–62.

[4] M.A. Rao, Rheology of Fluid, Semisolid, and Solid Foods: Principles and Applications, 3rd ed., Springer, Boston, MA, 2014.

[5] I. Filková, A.S. Mujumdar, Industrial spray drying systems, in: Arun S. Mujumdar (Ed.), Handbook of Industrial Drying, 4th ed., CRC Press, 2014, pp. 263–307.

[6] M. Diamantopoulos, C. Hochenauer, Atomizer design on pneumatic atomization in the high Ohnesorge number regime, Atomiz. Spr. 35 (2025) 41–61, https://doi.org/10.1615/AtomizSpr.2025061324.

[7] F.A. Hammad, K. Sun, Z. Che, J. Jedelsky, T. Wang, Internal two-phase flow and spray characteristics of outside-in-liquid twin-fluid atomizers, Appl. Therm. Eng. 187 (2021) 116555, https://doi.org/10.1016/j.applthermaleng.2021.116555.

[8] P. Stähle, J. Schröder, A. Kleinhans, H.P. Schuchmann, V. Gaukel, Effervescent atomization: a new atomizing technique for the energy-efficient spray drying of food liquids with high viscosity, Int. Dairy Magazine 8 (2013) 26–28, https://doi.org/10.5445/IR/1000051535.

[9] C. Anandharamakrishnan, S.P. Ishwarya, Spray Drying Technique For Food Ingredient Encapsulation, Wiley-Blackwell, IFT Press, Chichester, West Sussex ; Hoboken, NJ, 2015.

[10] P. Stähle, V. Gaukel, H.P. Schuchmann, Comparison of an effervescent nozzle and a proposed air-core-liquid-ring (ACLR) nozzle for atomization of viscous food liquids at low air consumption, J. Food Process. Eng. 40 (2017) 12268, https://doi.org/10.1111/jfpe.12268.

[11] M.O. Wittner, H.P. Karbstein, V. Gaukel, Spray performance and steadiness of an effervescent atomizer and an air-core-liquid-ring atomizer for application in spray drying processes of highly concentrated feeds, Chem. Eng. Process. - Process Intensific. 128 (2018) 96–102, https://doi.org/10.1016/j.cep.2018.04.017.

[12] M.A. Ballesteros Martínez, P. Roy, J.N. Solano Alarcón, V. Gaukel, Atomizing high-viscosity non-Newtonian fluids with the ACLR nozzle: correlation between internal flow and external spray instabilities, J. Nonnewton. Fluid. Mech. 338 (2025) 105405, https://doi.org/10.1016/j.jnnfm.2025.105405.

[13] M.A. Ballesteros Martínez, V. Gaukel, Using computation fluid dynamics to determine oil droplet breakup parameters during emulsion atomization with pressure swirl nozzles, Fluids 8 (2023) 277, https://doi.org/10.3390/fluids8100277.

[14] A. Mansour, N. Chigier, Air-blast atomization of non-Newtonian liquids, J. Nonnewton. Fluid. Mech. 58 (1995) 161–194, https://doi.org/10.1016/0377-0257(95)01356-Z.

[15] M.O. Wittner, H.P. Karbstein, V. Gaukel, Energy efficient spray drying by increased feed dry matter content: investigations on the applicability of Air-core-liquid-ring atomization on pilot scale, Dry. Technol. 38 (2020) 1323–1331, https://doi.org/10.1080/07373937.2019.1635616.

[16] M.R. Barbieri, U. Fritsching, Characterizing the internal flow behavior of spray pulsating operation in internal-mixing Y-jet atomizers, Fluids 11 (2025) 12, https://doi.org/10.3390/fluids11010012.

[17] D. Nam, S. Park, D. Kim, Experimental investigation on the spray characteristics of an internal-mixing twin-fluid nozzle in crossflow, Int. J. Multiphase Flow 194 (2026) 105461, https://doi.org/10.1016/j.ijmultiphaseflow.2025.105461.

[18] M.O. Wittner, M.A. Ballesteros, F.J. Link, H.P. Karbstein, V. Gaukel, Air-core–Liquid-ring (ACLR) atomization part II: influence of process parameters on the stability of internal liquid film thickness and resulting spray droplet sizes, Processes 7 (2019) 616, https://doi.org/10.3390/pr7090616.

[19] L. Qin, R. Yi, L. Yang, Theoretical breakup model in the planar liquid sheets exposed to high-speed gas and droplet size prediction, Int. J. Multiphase Flow 98 (2018) 158–167, https://doi.org/10.1016/j.ijmultiphaseflow.2017.09.010.

[20] M.A. Ballesteros Martínez, V. Gaukel, Spray drying of highly viscous feeds: modeling the internal flow of an ACLR atomizer for non-newtonian liquid feeds with high dry-matter contents, Dry. Technol. 43 (2025) 1824–1832, https://doi.org/10.1080/07373937.2025.2534037.

[21] A. Kumar, S. Sahu, Large scale instabilities in coaxial air-water jets with annular air swirl, Phys. Fluids 31 (2019) 124103, https://doi.org/10.1063/1.5122273.

[22] J. Schröder, A. Gunther, K.-E. Wirth, H.P. Schuchmann, V. Gaukel, Effervescent atomization of polyvinylpyrrolidone solutions: influence of liquid properties and atomizer geometry on liquid breakup and spray characteristics, Atomiz Spr. 23 (2013) 1–23, https://doi.org/10.1615/AtomizSpr.2013005849.

[23] M.O. Wittner, H.P. Karbstein, V. Gaukel, Air-core-liquid-ring (ACLR) atomization: influences of gas pressure and atomizer scale up on atomization efficiency, Processes 7 (2019) 139, https://doi.org/10.3390/pr7030139.

[24] M.A. Ballesteros Martínez, V. Gaukel, Time-averaged analysis and numerical modelling of the behavior of the multiphase flow and liquid lamella thickness inside an internal-mixing ACLR nozzle, Flow Turbulence Combust 110 (2023) 601–628, https://doi.org/10.1007/s10494-023-00406-5.

[25] M.O. Wittner, H. Karbstein, V. Gaukel, Pneumatic atomization: beam-steering correction in laser diffraction measurements of spray droplet size distributions, Appl. Sci. 8 (2018) 1738, https://doi.org/10.3390/app8101738.

[26] S. Sun, T. Zhang, Review of classical reservoir simulation. Reservoir Simulation: Machine Learning and Modeling, Gulf Professional Publishing, Cambridge, United States, 2020, pp. 23–86, https://doi.org/10.1016/B978-0-12-820957-8.00002-2.

[27] Siemens Industries Digital Software, Simcenter STAR-CCM+ User Guide, version 2206. https://plm.sw.siemens.com/en-US/simcenter/fluids-thermal-simulation/star-ccm/, 2022.

[28] C. Baker, T. Johnson, D. Flynn, H. Hemida, A. Quinn, D. Soper, M. Sterling, Train Aerodynamics, Butterworth-Heinemann, Oxford, 2019, https://doi.org/10.1016/C2016-0-04444-3.

[29] F. Nicoud, F. Ducros, Subgrid-scale stress modelling based on the square of the velocity gradient tensor, Flow Turbulence Combust 62 (1999) 183–200, https://doi.org/10.1023/A:1009995426001.

[30] M.A. Ballesteros Martínez, D. Becerra, V. Gaukel, Modelling the flow conditions and primary atomization of an air-core-liquid-ring (ACLR) atomizer using a coupled eulerian–Lagrangian approach, Flow Turbulence Combust 113 (2024) 437–458, https://doi.org/10.1007/s10494-024-00555-1.

[31] P.J. Carreau, Rheological equations from molecular network theories, Transac. Soc. Rheol. 16 (1972) 99–127, https://doi.org/10.1122/1.549276.

[32] K. Yasuda, R.C. Armstrong, R.E. Cohen, Shear flow properties of concentrated solutions of linear and star branched polystyrenes, Rheol. Acta 20 (1981) 163–178, https://doi.org/10.1007/BF01513059.

[33] M.A. Ballesteros Martínez, V. Gaukel, Understanding the operating limitations of an internal-mixing air-core-liquid-ring (ACLR) nozzle for process intensification in spray drying, Dry. Technol. 42 (2024) 2087–2094, https://doi.org/10.1080/07373937.2024.2328300.